

Simulations of transcatheter aortic valve implantation: implications for aortic root rupture

Qian Wang · Susheel Kodali · Charles Primiano · Wei Sun

Received: 5 January 2014 / Accepted: 29 March 2014 / Published online: 16 April 2014
© Springer-Verlag Berlin Heidelberg 2014

Abstract Aortic root rupture is one of the most severe complications of transcatheter aortic valve implantation (TAVI). The mechanism of this adverse event remains mostly unknown. The purpose of this study was to obtain a better understanding of the biomechanical interaction between the tissue and stent for patients with a high risk of aortic rupture. We simulated the stent deployment process of three TAVI patients with high aortic rupture risk using finite element method. The first case was a retrospective analysis of an aortic rupture case, while the other two cases were prospective studies, which ended with one canceled procedure and one successful TAVI. Simulation results were evaluated for the risk of aortic root rupture, as well as coronary artery occlusion, and paravalvular leak. For Case 1, the simulated aortic rupture location was the same as clinical observations. From the simulation results, it can be seen that the large calcified spot on the interior of the left coronary sinus between coronary ostium and the aortic annulus was pushed by the stent, causing the aortic rupture. For Case 2 and Case 3, predicated results from the simulations were presented to the clinicians at multidisciplinary pre-procedure meetings; and they were in agreement with clinician's observations and decisions. Our results indicated that the engineering analy-

sis could provide additional information to help clinicians evaluate complicated, high-risk aortic rupture cases. Since a systematic study of a large patient cohort of aortic rupture is currently not available (due to the low occurrence rate) to clearly understand underlying rupture mechanisms, case-by-case engineering analysis is recommended for evaluating patient-specific aortic rupture risk.

Keywords Patient-specific · Finite element · Aortic stenosis · Transcatheter aortic valve

1 Introduction

Since the first-in-man transcatheter aortic valve implantation (TAVI) was performed to treat aortic stenosis (AS) in 2002 (Cribier et al. 2002), more than 50,000 patients worldwide (Cribier 2012) have benefited from this revolutionary procedure. The results of the randomized PARTNER study in the USA recently confirmed the importance of TAVI in non-operable (Leon et al. 2010) and high-risk (Smith et al. 2011) patients. Recent studies also showed the promise of performing TAVI on lower-risk patients (Lange et al. 2011a).

Despite the clinical success, there are still many complications associated with TAVI. One of the most severe complications of TAVI is aortic root rupture (Eker et al. 2012; Hayashida et al. 2012; Lee et al. 2012; Pasic et al. 2012; Rezaq et al. 2012; Barbanti et al. 2013), which could lead to cardiac tamponade and subsequent fatal outcomes. Since aortic root rupture happens rarely [a reported risk of less than 2% (Lange et al. 2011b; Messika-Zeitoun et al. 2010; Barbanti et al. 2013)], it is difficult to identify its predictors. As a result, the mechanism of this adverse event remains largely unknown; and a better understanding of the biomechanical interaction between the aortic root and prosthesis is essential to prevent aortic root rupture in TAVI. The purpose of

Q. Wang · W. Sun (✉)

Tissue Mechanics Laboratory, The Wallace H. Coulter Department of Biomedical Engineering, Georgia Institute of Technology, Technology Enterprise Park Room 206, 387, Technology Circle, Atlanta, GA 30313-2412, USA
e-mail: wei.sun@bme.gatech.edu

S. Kodali

Center for Interventional Vascular Therapy, Columbia University College of Physicians and Surgeons, New York, NY 10032, USA

C. Primiano

Cardiology Department, The Hartford Hospital, Hartford, CT 06102, USA

this study was to perform an engineering finite element (FE) analysis of TAVI clinical cases, in order to obtain a better understanding of the biomechanical interaction between the tissue and stent for patients with a high risk of aortic rupture.

Computational analysis has been carried out to evaluate the aortic root—transcatheter aortic valve (TAV) interaction from an engineering perspective (Capelli et al. 2012; Wang et al. 2012; Auricchio et al. 2013; Gessat et al. 2014; Russ et al. 2013). However, the validity of the simulation results was limited by the assumptions of material properties and boundary conditions. For example, no material failure criteria were incorporated in the previous models. Hence, the injury to aortic root tissue, such as aortic root rupture, was not investigated. Moreover, the balloon expansion process was simplified by either forcing uniform TAV stent expansion in the radial direction or applying constant pressure to the balloon interior. The mechanics between balloon and TAV stent could not be accurately characterized.

In continuation of our previous research (Wang et al. 2012), we simulated the stent deployment process of three TAVI clinical patients with high aortic rupture risk. The first clinical case (Case 1) was a retrospective analysis of an actual TAVI aortic rupture case, while the other two cases were prospective studies of two high-risk cases, which, eventually, ended with one canceled procedure (Case 2) and one successful TAVI (Case 3). Dynamic structural FE models were created using patient-specific geometries segmented and reconstructed from patient preoperative CT scans, which incorporated aged human aortic material properties with material failure criteria obtained from mechanical tests. A surface-based fluid cavity method was utilized to simulate the fluid-filled TAVI balloon expansion process for the TAV stent deployment into patient-specific calcified aortic roots. Size 23 Edwards SAPIENT TAV stent, which is the currently approved device in the USA, was implanted in the three patients. Simulation results were evaluated for the risk of aortic root rupture, as well as coronary artery occlusion, and paravalvular leak.

2 Materials and methods

MSCT image acquisition Full phase cardiac MSCT scans (Fig. 1) were collected from patients at Columbia University Medical Center (New York, NY) and Hartford Hospital (Hartford, CT). Institutional Review Board approval to review patient images was obtained for the study. The MSCT examination was performed on a Toshiba 320-channel volume computed tomography scanner and a GE LightSpeed 64-channel volume computed tomography scanner.

Patient-specific aortic root model MSCT images in diastole were imported into Avizo 8.0 software (VSG, Burlington, MA) for three-dimensional (3D) reconstruction and eval-

uated using a window width of 950 and -50 Hounsfield units. Aortic root was identified and separated from the rest of the chest images to create a 3D representation (Wang et al. 2011). HyperMesh software (Altair Engineering, Inc., MI) was used to generate FE mesh of the 3D aortic root model (Fig. 2), which included aortic root, aortic leaflets, calcification, mitral–aortic intervalvular fibrosa, anterior mitral leaflet, fibrous trigones, and left ventricle. Three-dimensional solid elements (eight-node hexahedral C3D8I, six-node pentahedral C3D6, and four-node tetrahedral C3D4 elements) were used to simulate the TAVI cases in ABAQUS explicit 6.13 (SIMULIA, Providence, RI) FE software. Calcification (Fig. 2) was modeled such that the volume of 3D elements in HyperMesh was similar to that was quantified using the material statistics tool in Avizo. Calcification was quantified with density greater than 130 Hounsfield units.

Material models of heart tissues The anisotropic hyperelastic Holzapfel–Gasser–Ogden material model (Gasser et al. 2006) was adopted to characterize mechanical behaviors of the human heart tissues (i.e., aortic leaflets, aortic sinus, ascending aorta, mitral leaflet tissues, and myocardium). Briefly, the heart tissues are assumed to be composed of a matrix material with two families of embedded fibers, each of which has a preferred direction. The fiber directions (theta) can be mathematically described using two unit vectors. The strain invariant \bar{I}_1 is used to describe the matrix material; and the strain invariant \bar{I}_{4i} is used to describe the properties of the fiber families. \bar{I}_{4i} is equal to the squares of the stretches in the fiber directions. The strain energy function W can be expressed as

$$W = C_{10} \{ \exp [C_{01}(\bar{I}_1 - 3)] - 1 \} + \frac{k_1}{2k_2} \sum_{i=1}^2 \left[\exp \left\{ k_2 [\kappa \bar{I}_1 + (1 - 3\kappa) \bar{I}_{4i} - 1]^2 \right\} - 1 \right] + \frac{1}{D} (J - 1)^2, \quad i = 1, 2 \quad (1)$$

where, C_{10} , C_{01} , k_1 , k_2 and D are material constants. C_{10} and C_{01} are used to describe the matrix material. D is the material constant that introduces the near incompressibility, while k_1 is a positive material constant with the dimensions of stress and k_2 is a dimensionless parameter. In addition, a dispersion parameter κ was used to describe the distribution of fiber orientation. When $\kappa = 0$, the fibers are perfectly aligned (no dispersion). When $\kappa = 0.33$, the fibers are randomly distributed and the material becomes isotropic. Local coordinate systems were defined for each leaflet and sinus to include fiber orientations for each region.

The isotropic hyperelastic Ogden material model (Ogden 1972) was used to characterize the mechanical properties of the human mitral–aortic intervalvular fibrosa and fibrous trigones obtained from uniaxial testing. Aortic valve calcifi-

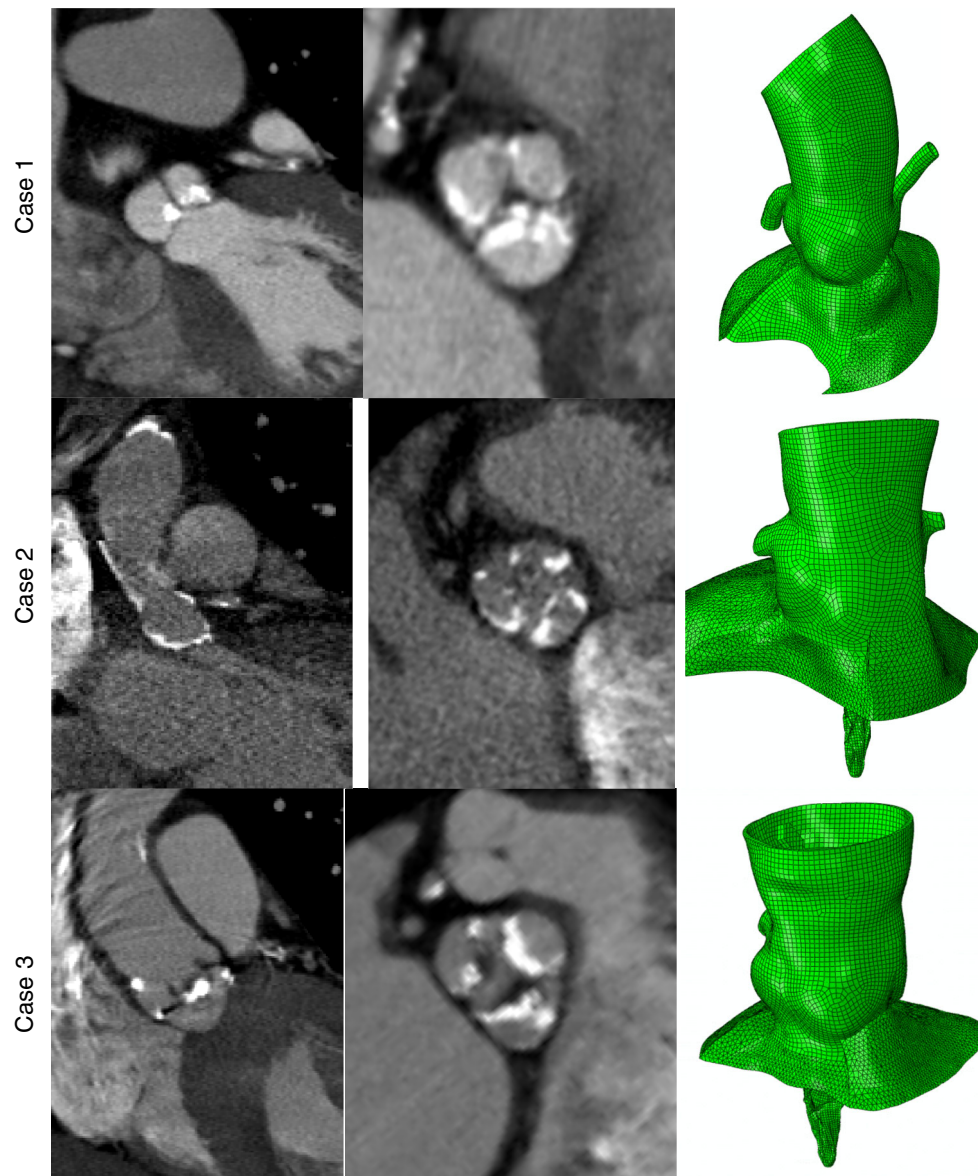


Fig. 1 MSCT images of the three stenotic aortic valves in long-axis and short-axis views and reconstructed aortic root models in ABAQUS

cation of the patients in this study had distinct and regional calcified tissue formations that can be observed from the MSCT images. Calcified tissues were assumed to be homogeneous and to have a Young's modulus of 12.6 MPa (Holzapfel et al. 2004) and a Poisson ratio of 0.3. To simulate the injury to the aortic root, material failure criterion was defined in the ABAQUS explicit user subroutine VUANISOHYPER by specifying a maximum principal stress limit of 2.5 MPa for the aortic sinuses. An element would be deleted from the FE model of the aortic root to simulate the rupture response, when the maximum principal stress was reached in all of the material points of the element. Details of the determination of material parameters for aged human heart tissues were described in previous publications (Martin et al. 2011; Mar-

tin and Sun 2012; Wang et al. 2012); and material parameters are listed in Table 1.

TAV stent geometry and material The stent model had a height of 14.3 mm and a thickness of 0.5 mm, which was generated using the depictions in the literature to closely resemble the Edwards Sapien stent geometry (Fig. 3). The stent was modeled with the properties of 316 stainless steel with a Young's modulus of 193 GPa, a Poisson ratio of 0.3, and initial yield stress of 340 MPa (Tzamtzis et al. 2013). The TAV leaflets were not included in the model because the effects of the TAV leaflets on biomechanical interaction between the TAV stent and aortic tissues during the stent expansion were assumed to be negligible. This assumption was based on the

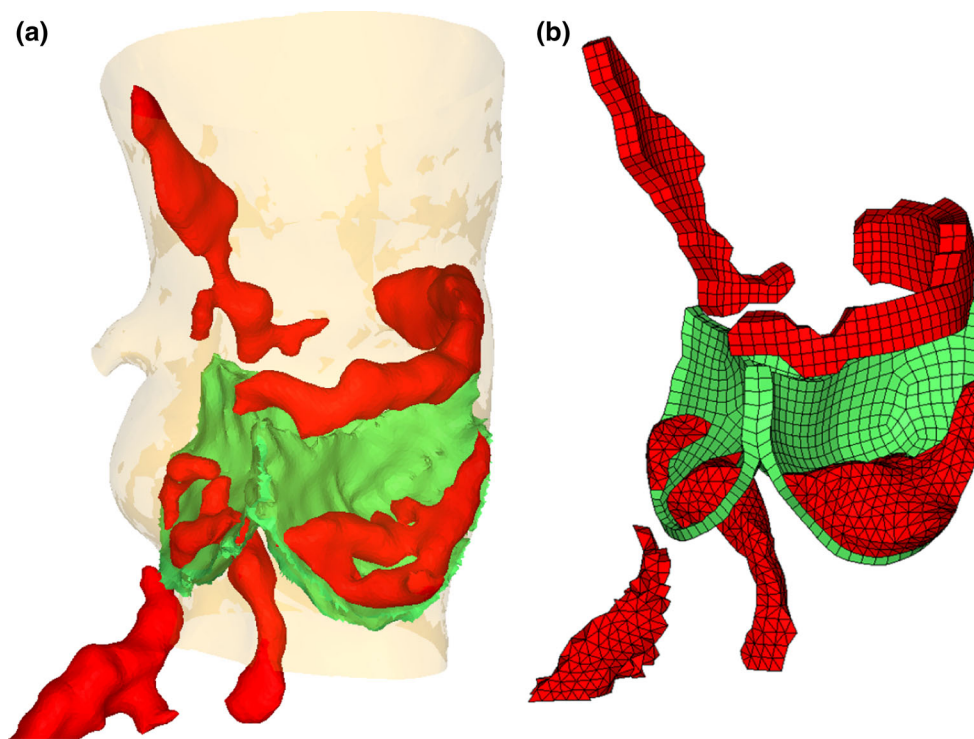


Fig. 2 The development of the aortic root model of Case 3: **a** initial image segmentation in Avizo, **b** reconstructed models of aortic leaflets and calcification. For illustration purposes, the yellow geometry in our

finite element models represents the aortic root, the green geometry represents non-calcified aortic leaflets, and the red geometry represents calcification

Table 1 Material parameters of non-calcified human aortic sinus, ascending aorta, leaflet, myocardium, anterior mitral leaflet, and mitral–aortic intervalvular fibrosa

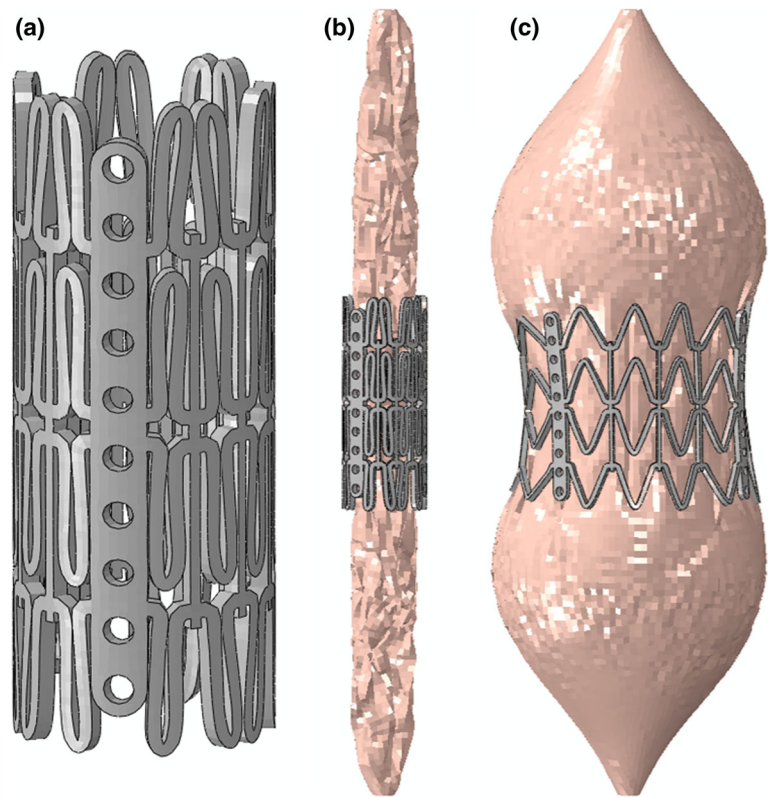
	C_{10}	C_{01}	K_1	K_2	κ	D	Theta(°)
Sinus	1.7553	13.7077	10.5507	80.3790	0.0006	0.0005	20.06
Ascending aorta	4.1755	3.4649	3.7711	15.9276	0.0864	0.0005	70.95
Leaflet	0.9627	6.3928	12.7250	48.6769	0.0711	0.0005	28.04
Myocardium	0.0374	15.3875	6.0798	98.3666	0.1440	0.0005	6.78
Mitral leaflet	0.1245	13.6655	11.0069	84.8478	0.0800	0.0005	13.09
	μ_1	α_1	μ_2	α_2	μ_3	α_3	
Fibrosa	2069.4	12.5	94.8	12.5	3182.6	12.5	

fact that TAV leaflets do not have direct contact with the native aortic tissue. Also, material properties of the TAV leaflets are significantly more compliant than those of the stainless steel stent. The pre-deployment geometry of the stent (Fig. 3a) was obtained by applying a displacement field outside in the radial direction to crimp the stent to an outside diameter of 7.3 mm.

Modeling of balloon deployment The mechanical response of a fluid-filled balloon expansion was modeled by a surface-based fluid cavity method in ABAQUS explicit, which was capable of simulating the coupling between the

deformation of the balloon and the fluid inside with uniform properties and state. Three-dimensional membrane elements (M3D4) were used to model a fully enclosed balloon, which resembled the Edwards RetroFlex three balloon geometry. The outer diameter, thickness, and total length of the balloon were 22, 0.06, and 63 mm, respectively. The balloon had a Young's modulus of 600 MPa and a Poisson ratio of 0.4 (Tzamtzis et al. 2013). The crimped balloon geometry (Fig. 3b) was obtained by applying a displacement field in the radial direction to a cylindrical crimper outside the balloon, to the extent that the balloon could fit inside the stent

Fig. 3 **a** Transcatheter aortic valve stent and **b** a realistic balloon used to simulate **c** fluid controlled balloon deployment



model. A total of 16 ml of water was used as the fluid to expand the balloon.

Simulation setup The dynamic balloon expansion process was simulated to complete in 1 s, which resulted in a constant flux rate of 16 ml/s. The top of the ascending aorta was constrained permitting only rotational degrees of freedom. Friction coefficient between TAV stents and stenotic aortic roots was assumed to be 0.1 based on the studies by (Mummert et al. 2013) and (Vad et al. 2010). Contact force between the stent and aortic root was output from ABAQUS and was calculated by summing the normal contact forces of the node set that represented the outside surface of the stent. Deformed geometry of the aortic root was used to examine the possible complications, such as aortic root rupture, coronary artery occlusion, and paravalvular leak.

3 Results

Case presentation Case 1 A 94-year-old female patient with a tricuspid aortic valve and an annulus size of 19.6 mm was referred for TAVI procedure. Echocardiography revealed severe AS in the non-coronary leaflet as well as the interior of the aortic root; only the left coronary leaflet could open during cardiac cycles. The pre-procedural MSCT scans (Fig. 1) showed heavy calcification on the non-coronary leaflet, and one large calcified spot on the interior of the left coronary

sinus at the level between the ostium of the left main stem and the aortic annulus entering the myocardium. A size 23 Edward SAPIEN TAV was implanted. During TAVI procedure, aortic root tearing happened and visualized below the left main coronary artery. **Case 2** Small and narrow left sinus of Valsalva was observed in a 65-year-old female patient with a tricuspid aortic valve and an annulus size of 23.7 mm (Fig. 1). Extensive aortic calcification was also present in the patient. The calcification on ascending aortic wall was extended into the sinuses and was joined with the calcification spots on aortic leaflets. Based on initial screening, the patient was considered as a borderline candidate to TAVI. FE analysis was performed before the scheduled TAVI operation; and the simulation results were presented to the clinicians and discussed at the pre-procedural meeting. Our simulation suggested a possibility of the left coronary artery occlusion and aortic root rupture. The patient was prepared and catheterized in the hybrid operating room and was further evaluated using echocardiography and angiography. On-site imaging assessments suggested high risk for the complication of both coronary artery occlusion and annulus rupture, which were generally in agreement with FE simulation results. The TAVI procedure was subsequently canceled. **Case 3** Severe calcification was observed in aortic leaflets, ascending aorta, and left ventricular outflow tract (LVOT) of an 80-year-old female patient with a tricuspid aortic valve and an annulus size of 19.7 mm (Fig. 1). The patient was referred for TAVI procedure. FE analysis was performed before the scheduled TAVI.

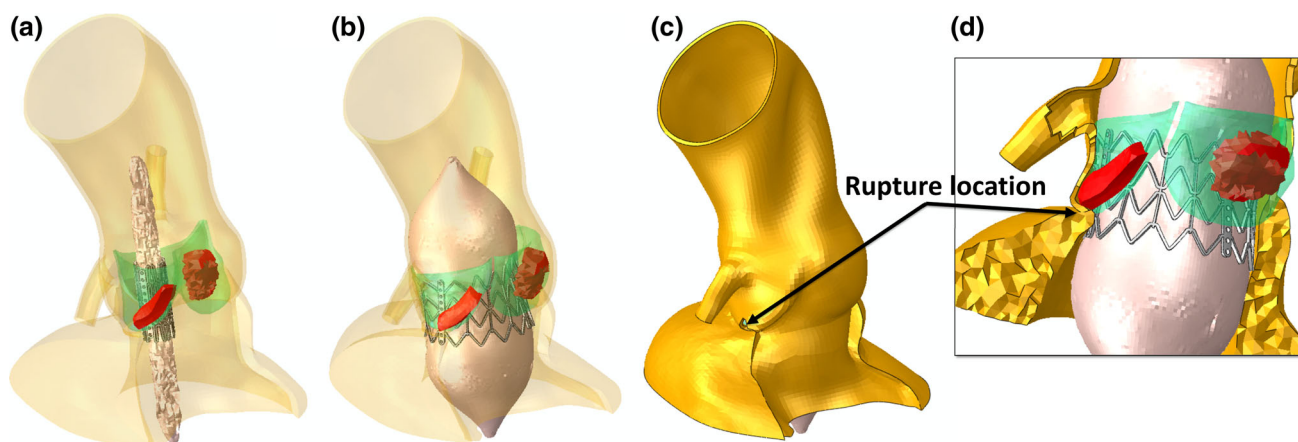


Fig. 4 **a** Pre- and **b** post-deployment geometries of the aortic root of Case 1. **c** Full and **d** local views of the deformed the aortic root and balloon deployment indicates annulus tearing under the left coronary ostium due to dislodgement of calcification into the vulnerable part of the aortic sinus

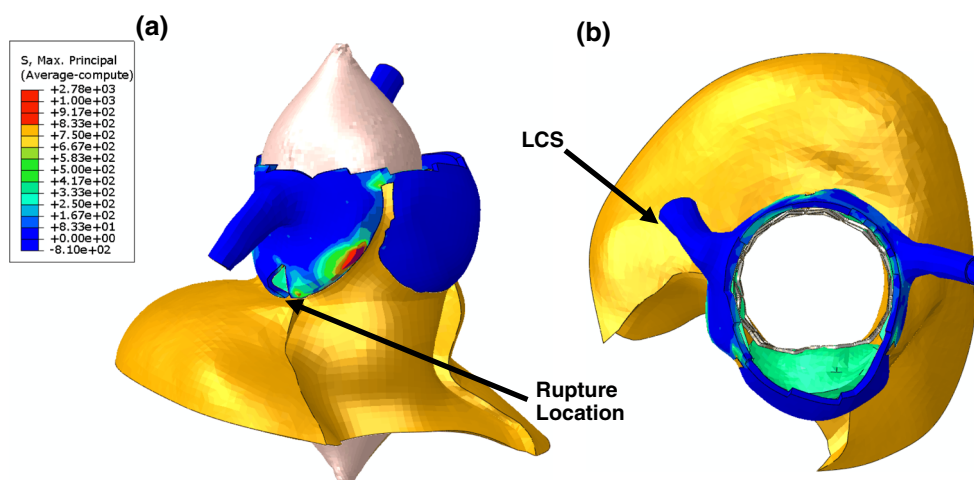


Fig. 5 Side **a** and top views **b** of the deformed native valve leaflets of Case 1 after the maximum stent deployment showed high stress at location of tearing. Stress (in kPa) contour plot was created for the aortic sinuses. *LCS* left coronary sinus

The simulation results indicated the possibility of a small paravalvular leak, but no complication of aortic rupture and coronary occlusion. Following the procedure a small paravalvular leak was observed in the patient; otherwise, TAVI procedure was successfully performed.

Simulation results The deformed aortic roots after the maximum stent deployment are shown in Figs. 4, 5 and 6.

Case 1 The simulation of the TAVI procedure revealed that asymmetric distribution of the aortic calcification lead to asymmetric expansion of the TAV stent with respect to the center of the aortic root. The TAV stent in the non-coronary sinus region was partially expanded, compared to fully expanded stent in the less calcified left coronary sinus region. The calcified spot on the interior of the left coronary sinus was displaced by the TAV stent (Fig. 4), causing stress concentration at the bottom of the left coronary sinus (Fig. 5) and consequently the aortic rupture. High stress and

strain were generally observed at the aortic tissue where it contacted the calcification and stent struts. Contact radial force between the TAV stent and aortic root reached 137.5 N, when the stent was fully deployed. Rupture of the aortic root at the bottom of the left coronary sinus occurred at roughly 82 % of the balloon volume. The balloon pressure at full deployment was 3.5 atm. Rupture location in the simulation was the same as that in the clinical case.

Case 2 The simulation results showed that the TAV stent was expanded uniformly inside the aortic valve. During the balloon deployment, the extensive calcification along the aortic wall at the level of the ascending aortic and sinuses lead to non-uniform deformation of the aortic sinus tissue in the circumferential direction. Additionally, although the annulus size of the patient was slightly larger than the TAV stent, the sinuses of Valsalva of the patient were small and flat, which implied that the sinuses had very little room for the displacement of the native calcified leaflets during expansion.

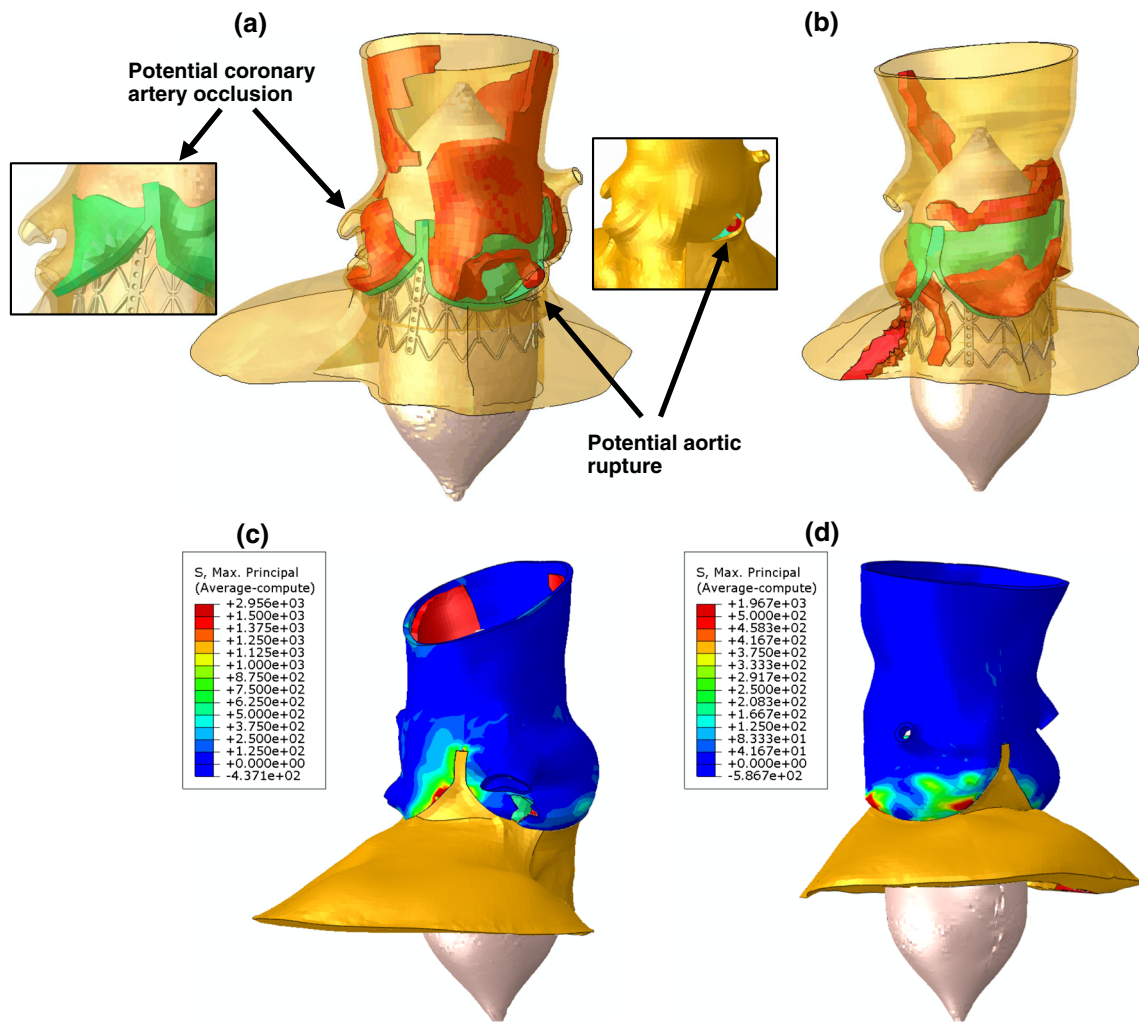


Fig. 6 Post-deployment geometries and stress (in kPa) contour plots of the aortic roots of (a, c) Case 2; and (b, d) Case 3 were utilized to evaluate the potential of complications such as aortic root rupture, coronary

artery occlusion, and paravalvular leak. Stress (in kPa) contour plots (c, d) were created for the aortic sinuses

sion. As a result, rupture was observed at the bottom of each sinus where it was in contact with calcification spots. Rupture of the aortic root at the bottom of the left coronary sinus started at approximately 88 % of the planned balloon injection volume (Fig. 6a). Additionally, the deformed geometry showed that the native left coronary leaflet could cause possible coronary artery occlusion (Fig. 6a). Contact force between the tissue and device in the normal direction was 41.3 N at the end of the simulation, while the balloon pressure was 3.0 atm.

Case 3 The simulation results indicated that the TAV stent was expanded fully inside the aortic valve. A small paravalvular leak was observed at the bottom of the left coronary leaflet where a LVOT calcification spot was present (Fig. 7). No other complication was observed from the simulation results. Contact force between the TAV stent and aortic root in the

normal direction was 113.0 N at full deployment, while the balloon pressure was 3.8 atm.

4 Discussions

Potential mechanisms of the aortic root rupture The common practice of oversizing of the TAV stent, which is used to reduce the risk of the paravalvular leak (Samim et al. 2012; Berdajs 2013), could lead to the aortic root rupture. In other studies (Pasic et al. 2012; Barbanti et al. 2013), heavily calcified aortic annulus, LVOT, and leaflets, a narrow or calcified aortic root, enhanced oval shape of the annulus were also identified as anatomic factors that could be responsible for aortic rupture. In the study by (Hayashida et al. 2012), it was hypothesized that the epicardial fat segment might be a

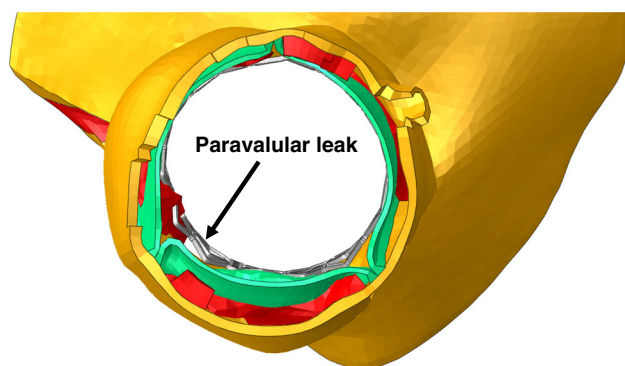


Fig. 7 Top view of the deformed native valve leaflets of Case 3 after the maximum stent deployment showed a small paravalvular leak

vulnerable area, since this part of the aortic annulus is not covered by cardiac structures and is directly adjacent to the epicardial fat and pericardial cavity. Therefore, it was conjectured that annulus rupture was caused by forceful expansion of the TAV stent and subsequent dislodgement of calcification into the vulnerable part of the sinus which lacked support of cardiac structure.

For Case 1 in our study, one large calcification was observed on the interior of the left coronary sinus under the left coronary ostium, which was similar to the rupture cases described by (Hayashida et al. 2012). By using FE analysis to virtually replicate and visualize the TAV stent expansion process, it can be clearly seen that the large calcified spot on the interior of the left coronary sinus between coronary ostium and the aortic annulus was pushed by the stent, causing the aortic rupture. Thus, the aortic root rupture of Case 1 could be caused by a combination of two factors: (a) the large calcified spot on the interior of the left coronary sinus and near the aortic annulus and (b) the asymmetric distribution of the aortic calcification due to a significantly large calcification on the non-coronary leaflet.

However, compared to Case 1, Case 2 and Case 3 presented two different patient anatomy and calcification configurations. For Case 2, our simulation results predicted the potential aortic rupture due to the flat- and narrow-shaped sinuses of Valsalva and the heavy calcification on the aortic wall and valve. For Case 3, even though aortic leaflets were heavily calcified and isolated calcification was present in the LVOT, the aortic sinuses were mostly calcification free. Calcified native leaflets were able to be displaced into the curved sinuses of Valsalva during expansion. Subsequently, TAVI could be performed successfully without any major complications. For the analysis of the three cases, it can be seen that multiply patient factors and/or a combination of them could be the cause of aortic root rupture. The patient factors could include the individual patient aortic tissue geometries and material properties, as well as calcification volume, shape, location, and orientation.

TAV sizing directly affects contact forces between the stent and the calcified aortic root. TAV sizing has been identified as one of the key indicators of aortic rupture (Barbanti et al. 2013; Pasic et al. 2012). From our simulation results, it can be seen that there was a difference in balloon pressure and contact normal forces between the three patients in this study, and the pressure and force values were not correlated with the aortic rupture results. Indeed, in the study by (Barbanti et al. 2013), rupture happened even when aortic valve was under-sized (Patient 18 of the study had a relative area oversizing of -2.58% , while Patient 5 and Patient 19 only had roughly 2% oversizing). Similarly, comparison of Case 1 and Case 3 of the current study showed that TAVI clinical results could be very different even if the annulus size (19.6 vs. 19.7 mm) and selected device (both 23 Sapien valves) were the same. Clearly, TAV sizing should be evaluated with patient-specific anatomic features and calcification configurations, which underscored the importance of *patient-specific* analysis of complicated, rare clinical TAVI cases of aortic rupture.

Different methods of modeling of balloon deployment In this study, balloon expansion process was simulated using a surface-based fluid cavity method. Previously, the balloon expansion process was simplified by either forcing uniform stent expansion in the radial direction or applying constant pressure to the balloon interior (Beule et al. 2008; Gervaso et al. 2008; Lim et al. 2008; Pasic et al. 2012; Capelli et al. 2010). Although using uniform radial displacement could guarantee the stent to expand precisely to a desired diameter, the limitation was that the stent would not be able to deform, which implied that the simulation results could overestimate the stent force exerted on the tissue as well as the tissue deformation. Other researchers reported the foreshortening and dogboning shapes produced by using constant pressure. However, the challenge of this method was the determination of the applied pressure that could precisely expand the stent to a desired diameter, since the compliance/stenotic condition could vary between patients. In reality, when the TAV balloon is prepared, the inflation device is filled with a define volume which will produce either 23 or 26 mm of balloon expansion. During the TAV implantation procedure, the entire volume in the inflation device is delivered to the balloon independent of the pressure. The fluid cavity method used in this study overcame the assumptions of the previous balloon models and was able to characterize the real balloon expansion phenomenon.

Limitations of the model There are many assumptions and limitations in this study. Our simulation results should be interpreted with the consideration of these assumptions and limitations. First, only three TAVI clinical cases were investigated in this paper, and more prospective clinical cases are

needed to validate our modeling methods. In the model setup, we assumed that the TAV stent was deployed at the optimal height and implantation angle. The impact of different stent deployment heights and implantation angles will be studied in the future. There is a lack of studies on the material properties of the aortic valve calcification (Ebenstein et al. 2009; Holzapfel et al. 2004; Jeziorska et al. 1998). Therefore, a parametric study may be necessary to investigate the effects of calcification stiffness on biomechanical interaction during TAVI. Similarly, there is a lack of the data on the material properties, including ultimate tensile strength (UTS), of human aortic sinuses in the literature. Based on our preliminary data from uniaxial tests on aortic tissue, the UTS of the aortic sinuses was found to be in the range from 2.3 to 3.1 MPa. A maximum principal stress limit of 2.5 MPa was used as the material failure limit for the aortic sinuses. Since material properties of human aortic tissues could be different even among patients with same age and gender, in order to provide a confidence interval for the simulation results, more material tests on human aortic root tissue should be conducted in future studies. Furthermore, experimental tests will be performed to validate the fluid controlled balloon model. No blood flow was considered in the current study. Therefore, paravalvular leak and coronary occlusion were evaluated by examining the deformed geometries of the stent and tissue.

5 Conclusions

We presented patient-specific FE models of three TAVI clinical cases, which incorporated human aortic tissue material properties with material failure criteria, and balloon expansion process using a surface-based fluid cavity method. Simulation results indicated that aortic rupture mechanism was complicated and could be different among patients. We demonstrated that the engineering analysis could provide additional information to help clinicians evaluate complicated, high-risk aortic rupture cases. Since a systematic study of a large patient cohort of aortic rupture is currently not available (due to the low occurrence rate) to clearly understand underlying rupture mechanisms, case-by-case engineering analysis would be particularly helpful for evaluating patient-specific aortic rupture risk.

Acknowledgments This work was supported in part by NIH HL104080, HL108239 grants, and AHA predoctoral fellowship 13PRE148300-02. We would like to thank Dr. Raymond McKay at the Hartford Hospital, CT for providing the image data. We would also like to thank Caitlin Martin, Thuy Pham, and Kewei Li for providing experimental data of the heart tissues, and technical support provided by Dura Biotech.

Conflict of interest All authors disclose any financial and personal relationships with other people or organizations that could inappropriately influence (bias) their work.

References

- Auricchio F, Conti M, Morganti S, Reali A (2013) Simulation of transcatheter aortic valve implantation: a patient-specific finite element approach. *Comput Methods Biomech Biomed Eng*. doi:[10.1080/10255842.2012.746676](https://doi.org/10.1080/10255842.2012.746676)
- Barbanti M, Yang TH, Tamburino C, Wood DA, Jiliahawi H, Blanke P, Makkar RR, Latib A, Colombo A, Tarantini G, Raju R, Binder RK, Nguyen G, Freeman M, Ribeiro HB, Kapadia S, Min J, Feuchter G, Gurtvich R, Alqoofi F, Pelletier M, Ussia GP, Napodano M, de Brito FS, Kodali S Jr, Norgaard BL, Hansson NC, Pache G, Canovas SJ, Zhang H, Leon MB, Webb JG, Leipsic J (2013) Anatomical and procedural features associated with aortic root rupture during balloon-expandable transcatheter aortic valve replacement. *Circulation* 128(3):244–253. doi:[10.1161/CIRCULATIONAHA.113.002947](https://doi.org/10.1161/CIRCULATIONAHA.113.002947)
- Berdajs D (2013) Aortic root rupture: implications of catheter-guided aortic valve replacement. *Curr opin cardiol* 28(6):632–638. doi:[10.1097/HCO.0b013e3283655bb5](https://doi.org/10.1097/HCO.0b013e3283655bb5)
- Capelli C, Bosi GM, Cerri E, Nordmeyer J, Odenwald T, Bonhoeffer P, Migliavacca F, Taylor AM, Schievano S (2012) Patient-specific simulations of transcatheter aortic valve stent implantation. *Med Biol Eng Comput* 50(2):183–192
- Capelli C, Nordmeyer J, Schievano S, Lurz P, Khambadkone S, Lattanzio S, Taylor AM, Petrini L, Migliavacca F, Bonhoeffer P (2010) How do angioplasty balloons work: a computational study on balloon expansion forces. *Eurointervention* 6(5):638–642
- Cribier A (2012) Development of transcatheter aortic valve implantation (TAVI): A 20-year odyssey. *Arch Cardiovasc Dis* 105(3):146–152. doi:[10.1016/j.acvd.2012.01.005](https://doi.org/10.1016/j.acvd.2012.01.005)
- Cribier A, Eltchaninoff H, Bash A, Borenstein N, Tron C, Bauer F, Derumeaux G, Anselme F, Laborde F, Leon MB (2002) Percutaneous transcatheter implantation of an aortic valve prosthesis for calcific aortic stenosis: first human case description. *Circulation* 106(24):3006–3008
- De Beule M, Mortier P, Carlier SG, Verhegghe B, Van Impe R, Verdonck P (2008) Realistic finite element-based stent design: the impact of balloon folding. *J Biomech* 41(2):383–389
- Ebenstein DM, Coughlin D, Chapman J, Li C, Pruitt LA (2009) Nanomechanical properties of calcification, fibrous tissue, and hematoma from atherosclerotic plaques. *J Biomed Mater Res A* 91(4):1028–1037
- Eker A, Sozzi FB, Civaia F, Bourlon F (2012) Aortic annulus rupture during transcatheter aortic valve implantation: safe aortic root replacement. *Eur J Cardiothorac Surg* 41(5):1205. doi:[10.1093/ejcts/ezr146](https://doi.org/10.1093/ejcts/ezr146)
- Gasser TC, Ogden RW, Holzapfel GA (2006) Hyperelastic modelling of arterial layers with distributed collagen fibre orientations. *J R Soc Interface* 3(6):15–35
- Gervaso F, Capelli C, Petrini L, Lattanzio S, Di Virgilio L, Migliavacca F (2008) On the effects of different strategies in modelling balloon-expandable stenting by means of finite element method. *J Biomech* 41(6):1206–1212. doi:[10.1016/j.jbiomech.2008.01.027](https://doi.org/10.1016/j.jbiomech.2008.01.027)
- Gessat M, Hopf R, Pollok T, Russ C, Frauenfelder T, Sundermann SH, Hirsch S, Mazza E, Szekeley G, Falk V (2014) Image-based mechanical analysis of stent deformation: concept and exemplary implementation for aortic valve stents. *IEEE Trans Biomed Eng* 61(1):4–15. doi:[10.1109/TBME.2013.2273496](https://doi.org/10.1109/TBME.2013.2273496)
- Hayashida K, Bouvier E, Lefevre T, Hovasse T, Morice MC, Chevalier B, Romano M, Garot P, Farge A, Donzeau-Gouge P, Cormier B (2012) Potential mechanism of annulus rupture during transcatheter aortic valve implantation. *Catheter Cardiovasc Interv*. doi:[10.1002/ccd.24524](https://doi.org/10.1002/ccd.24524)
- Holzapfel GA, Sommer G, Regitnig P (2004) Anisotropic mechanical properties of tissue components in human atherosclerotic plaques. *J Biomech Eng* 126(5):657–665

- Jeziorska M, McCollum C, Wooley DE (1998) Observations on bone formation and remodelling in advanced atherosclerotic lesions of human carotid arteries. *Virchows Arch* 433(6):559–565
- Lange R, Bleiziffer S, Mazzitelli D, Elhmidi Y, Opitz A, Krane M, Deutsch MA, Ruge H, Brockmann G, Voss B, Schreiber C, Tassani P, Piazza N (2011a) Improvements in transcatheter aortic valve implantation outcomes in lower surgical risk patients: a glimpse into the future. *J Am Coll Cardiol* 59(3):280–287
- Lange R, Bleiziffer S, Piazza N, Mazzitelli D, Hutter A, Tassani-Prell P, Laborde JC, Bauernschmitt R (2011b) Incidence and treatment of procedural cardiovascular complications associated with transarterial and trans-apical interventional aortic valve implantation in 412 consecutive patients. *Eur J Cardiothorac Surg* 40(5):1105–1113
- Lee L, Henderson R, Baig K (2012) Successful treatment of aortic root rupture following transcatheter aortic valve implantation in a heavily calcified aorta: A novel approach to a serious complication. *Catheter Cardiovasc Interv*. doi:10.1002/ccd.24468
- Leon MB, Smith CR, Mack M, Miller DC, Moses JW, Svensson LG, Tuzcu EM, Webb JG, Fontana GP, Makkar RR, Brown DL, Block PC, Guyton RA, Pichard AD, Bavaria JE, Herrmann HC, Douglas PS, Petersen JL, Akin JJ, Anderson WN, Wang D, Pocock S, Investigators PT (2010) Transcatheter aortic-valve implantation for aortic stenosis in patients who cannot undergo surgery. *N Engl J Med* 363(17):1597–1607
- Lim D, Cho SK, Park WP, Kristensson A, Ko JY, Al-Hassani ST, Kim HS (2008) Suggestion of potential stent design parameters to reduce restenosis risk driven by foreshortening or dogboning due to non-uniform balloon-stent expansion. *Ann Biomed Eng* 36(7):1118–1129
- Martin C, Pham T, Sun W (2011) Significant differences in the material properties between aged human and porcine aortic tissues. *Eur J Cardiothorac Surg* 40(1):28–34
- Martin C, Sun W (2012) Biomechanical characterization of aortic valve tissue in humans and common animal models. *J Biomed Mater Res A* 100(6):1591–1599. doi:10.1002/jbm.a.34099
- Messika-Zeitoun D, Serfaty JM, Brochet E, Ducrocq G, Lepage L, Detaint D, Hyafil F, Himbert D, Pasi N, Laissy JP, Lung B, Vahanian A (2010) Multimodal assessment of the aortic annulus diameter: implications for transcatheter aortic valve implantation. *J Am Coll Cardiol* 55(3):186–194. doi:10.1016/j.jacc.2009.06.063
- Mummert J, Sirois E, Sun W (2013) Quantification of biomechanical interaction of transcatheter aortic valve stent deployed in porcine and ovine hearts. *Ann Biomed Eng* 41(3):577–586. doi:10.1007/s10439-012-0694-1
- Ogden RW (1972) Large deformation isotropic elasticity—on the correlation of theory and experiment for incompressible rubberlike solids. *Proc R Soc Lond A* 326(1567):565–584. doi:10.1098/rspa.1972.0026
- Pant S, Bressloff NW, Limbert G (2012) Geometry parameterization and multidisciplinary constrained optimization of coronary stents. *Biomech Model Mechanobiol* 11(1–2):61–82. doi:10.1007/s10237-011-0293-3
- Pasic M, Unbehaun A, Dreysse S, Buz S, Drews T, Kukucka M, D’Ancona G, Seifert B, Hetzer R (2012) Rupture of the device landing zone during transcatheter aortic valve implantation: a life-threatening but treatable complication. *Circ Cardiovasc Interv* 5(3):424–432. doi:10.1161/CIRCINTERVENTIONS.111.967315
- Rezq A, Basavarajaiah S, Latib A, Takagi K, Hasegawa T, Figini F, Cioni M, Franco A, Montorfano M, Chieffo A, Maisano F, Corvaja N, Alfieri O, Colombo A (2012) Incidence, management, and outcomes of cardiac tamponade during transcatheter aortic valve implantation: a single-center study. *JACC Cardiovasc Interv* 5(12):1264–1272. doi:10.1016/j.jcin.2012.08.012
- Russ C, Hopf R, Hirsch S, Sundermann S, Falk V, Szekely G, Gessat M Simulation of transcatheter aortic valve implantation under consideration of leaflet calcification. In: Engineering in Medicine and Biology Society (EMBC), 2013 35th Annual International Conference of the IEEE, 3–7 July 2013 2013. pp 711–714. doi:10.1109/EMBC.2013.6609599.
- Samim M, Stella PR, Agostoni P, Kluin J, Ramjankhan F, Sieswerda G, Budde R, van der Linden M, Juthier F, Banfi C, Hurt C, Hillaert M, van Herwerden L, Bertrand ME, Doevendans PA, Van Belle E (2012) A prospective “oversizing” strategy of the Edwards SAPIEN bioprosthesis: Results and impact on aortic regurgitation. *J Thorac Cardiovasc Surg*. doi:10.1016/j.jtcvs.2011.12.067
- Smith CR, Leon MB, Mack MJ, Miller DC, Moses JW, Svensson LG, Tuzcu EM, Webb JG, Fontana GP, Makkar RR, Williams M, Dewey T, Kapadia S, Babaliaros V, Thourani VH, Corso P, Pichard AD, Bavaria JE, Herrmann HC, Akin JJ, Anderson WN, Wang D, Pocock SJ (2011) Transcatheter versus surgical aortic-valve replacement in high-risk patients. *N Engl J Med* 364(23):2187–2198. doi:10.1056/NEJMoa1103510
- Tzamtzis S, Viquerat J, Yap J, Mullen MJ, Burriesci G (2013) Numerical analysis of the radial force produced by the Medtronic–CoreValve and Edwards-SAPIEN after transcatheter aortic valve implantation (TAVI). *Med Eng Phys* 35(1):125–130. doi:10.1016/j.medengphy.2012.04.009
- Vad S, Eskinazi A, Corbett T, McGloughlin T, Vande Geest JP (2010) Determination of coefficient of friction for self-expanding stent-grafts. *J Biomech Eng* 132(12):121007
- Wang Q, Book G, Primiano C, McKay R, Kodali S, Sun W (2011) Dimensional analysis of aortic root geometry during diastole using 3D models reconstructed from clinical 64-slice computed tomography images. *Cardiovasc Eng Technol* 2(4):324–333. doi:10.1007/s13239-011-0052-8
- Wang Q, Sirois E, Sun W (2012) Patient-specific modeling of biomechanical interaction in transcatheter aortic valve deployment. *J Biomech* 45(11):1965–1971. doi:10.1016/j.jbiomech.2012.05.008